Organic & Biomolecular Chemistry

PAPER

View Article Online
View Journal | View Issue

Cite this: *Org. Biomol. Chem.*, 2017, **15**, 10281

"Snorkelling" *vs.* "diving" in mixed micelles probed by means of a molecular bathymeter†

Gemma M. Rodriguez-Muñiz, [a] Miguel Gomez-Mendoza, [a] Edurne Nuin, [a] Inmaculada Andreu, [a,b] M. Luisa Marin *[a] and Miguel A. Miranda *[a]

Received 21st October 2017,
Accepted 22nd November 2017

DOI: 10.1039/c7ob02595e

rsc.li/obc

A photoactive bathymeter based on a carboxylic acid moiety covalently linked to a signalling methoxynaphthalene (MNP) fluorophore has been designed to prove the concept of "snorkelling" *vs.* "diving" in mixed micelles (MM). The carboxylic acid "floats" on the MM surface, while the MNP unit sinks deep in MM. The rate constants of MNP fluorescence quenching by iodide, which remains basically in water, consistently decrease with increasing spacer length, revealing different regions. This is associated with the distance MNP should "dive" in MM to achieve protection from aqueous reactants. Unequivocal proof of the exergonic photoinduced electron transfer was obtained from the UV-visible spectral signature of I_3^- upon steady-state photolysis. The applicability of the bathymeter was examined upon testing a family of MNP derivatives. The obtained results were validated by comparison with different lipophilicity tests: (i) a modified version of the K_{ow} partition coefficient and (ii) the retention factor on thin layer chromatography. This concept could potentially be extended to test drugs or pharmacophores exhibiting any photoactive moiety.

Introduction

Mixed micelles (MM) made of bile salts, phospholipids and cholesterol (Ch) are among the most important biological entities in mammals, exhibiting, for instance, an outstanding capability for solubilizing lipophilic molecules.[1,2] More specifically, MM play a pivotal role in maintaining Ch at an appropriate concentration in the blood stream.[3,4] Moreover, the lipophilic microenvironment provided by MM can be exploited for the development of pharmaceutical formulations, with an improved delivery into the target along with a decreased toxicity.[5–7]

Lipophilicity and membrane partition properties of potential drug candidates are key to the recognition of their target.[8,9] In this context, the position of small peptides and other molecules in membrane model systems has been assessed by the chemical shift perturbation experienced by the ^{13}C NMR spectra.[10] Further studies have qualitatively determined the location of different compounds within lipid bilayers by ^{13}C NMR chemical shift polarity correlation.[11] The obtained results have been useful to design a "molecular ruler" correlating polarity data with distances from the aqueous phase to quantitatively locate the penetration depth of intercalants within lipid bilayers,[12–14] eventually complemented with fluorescence measurements.[15] Furthermore, in connection with the role of biological membranes in radical attack, the depth of radical penetration in different kinds of membranes has been studied by ESR using spin traps.[16] In this context, the relationship between antioxidant capability and hydrophobicity in emulsions follows a non-linear trend explained by the so-called "cut-off effect" generally observed in cultured cells.[17–21]

Photodynamic therapy to eradicate cancer cells is based on the generation of singlet oxygen by a sensitizer.[22–25] As the potential activity of singlet oxygen is limited by diffusion to the aqueous phase, its generation at a deeper position in the bilayer could, in principle, result in a greater efficiency. This has been demonstrated in lipid membranes of lecithin liposomes by increasing the vertical porphyrin depth in the membrane bilayer,[26,27] which results in a decrease in the chromophore emission intensity upon quenching by iodide.[28]

Recently, we have developed photoactive probes with a covalently attached dansyl or methoxynaphthalene (MNP) label, to monitor the incorporation of Ch into MM by means of photophysical techniques.[29] Moreover, efficient encapsulation of the currently administered drugs (*S*)-naproxen, (*R*)-cinacalcet and (*S*)-propranolol into MM has been demonstrated by time-resolved fluorescence and laser flash photolysis.[30]

[a]*Instituto Universitario Mixto de Tecnología Química (UPV-CSIC) Universitat Politècnica de València, Avda de los Naranjos s/n, 46022 Valencia, Spain*
[b]*Instituto de Investigación Sanitaria (IIS)-La Fe, Hospital Universitari i Politècnic La Fe, Avda Fernando Abril Martorell 106, 46026 Valencia, Spain.*
E-mail: mmiranda@qim.upv.es, marmarin@qim.upv.es; Fax: (+) 0034963877809

†Electronic supplementary information (ESI) available. See DOI: 10.1039/c7ob02595e

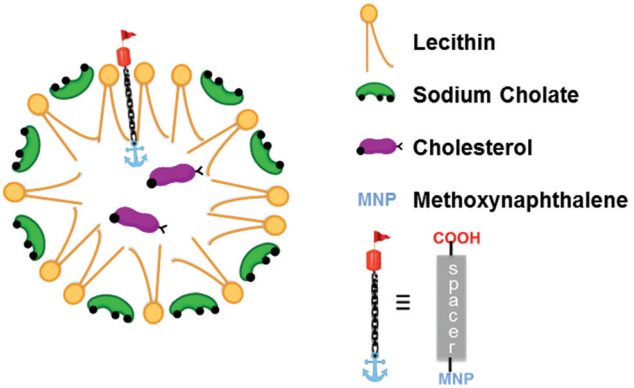

Fig. 1 Cartoon representation of the photoactive probes with different spacer lengths anchored to the surface by the acid while maintaining the chromophore diving as far as allowed inside MM.

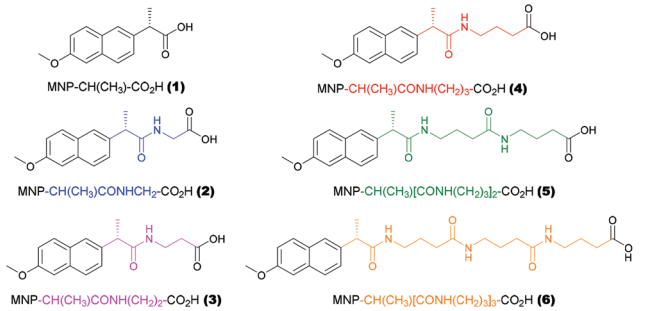

Chart 1 Chemical structures of the new photoactive MNP derivatives.

Interestingly, a remarkable decrease in the quenching rate constants of their excited states, either singlet or triplet, by ionic species is found upon the entrapment of the drugs inside these supramolecular entities.

With this background, we have now envisaged the possibility of designing and testing a photoactive bathymeter based on a carboxylic acid tail end, to ensure floating on the MM surface, and a signalling MNP at a fixed distance, to reveal "snorkelling" *versus* "diving" inside MM (Fig. 1). The selected MM appear particularly suitable for this purpose. This is because they are monolayered microheterogeneous systems with a relatively large size (10–100 nm)[29] that defines two lipophilic regions, corresponding to the phospholipidic shell (snorkelling region) and the strongly lipophilic Ch-containing core (diving region).

Thus, the as-built photoactive bathymeter was expected to report on the increasing depth of MNP-containing compounds in MM and on the changes in chemical reactivity associated with this parameter. This concept could potentially be extended to test drugs or pharmacophores exhibiting any photoactive chromophore.

Results and discussion

A family of new methoxynaphthalene derivatives was synthesized from (*S*)-naproxen (**1**) (see Chart 1 for the synthesis and pages S2–S27 of the ESI† for detailed spectroscopic characterization). The distances between the carboxylic acid and the MNP unit in **1–6**, estimated as a number of spacer bonds, were two, five, six, seven, twelve and seventeen, respectively. According to simple molecular modelling estimations (Chem BioDraw Ultra 13.0), they correspond to 25, 48, 63, 72, 95 and 148 nm, respectively. Subsequent formation of MM and encapsulation of the MNP derivatives were achieved in one pot following our recently reported procedure.[30] Briefly, a methanolic solution of the corresponding MNP probe was added to a methanol/dichloromethane solution of lecithin, sodium cholate and Ch. After evaporation of the solvent, rehydration of the resulting film led to MM containing the photoactive unit soaked. It is worth noting that no significant changes were observed in the shapes and emission intensities (λ_{max} = 353 nm, Φ_F = 0.39)[31] or even in the singlet lifetimes (τ_s *ca.* 10 ns) of the MNP derivatives as a result of their incorporation into MM. This fact reveals that the singlet excited state of this particular chromophore, in the absence of a quencher, is not sensitive to the environment hydrophobicity.

Quenching experiments using iodide were performed to investigate on the protection of MM from a reactant in the aqueous phase. Thus, quenching of the fluorescence of **1–6** by iodide, under steady-state and time-resolved conditions, was performed in MM and the results were compared to the ones achieved in solution (Fig. 2A for **1** and 2B for **6** as representative examples, additional information can be found in the ESI, pages S28 and 29†). In all cases, the quenching plots yielded good linear fits, which proves that the MNP derivatives are homogeneously distributed within MM.

The results obtained for **1** (shortest distance from MNP to the surface) clearly show that the slope of the corresponding Stern–Volmer plots in MM is only half of the value found in solution. On the other hand, Fig. 2B shows the results for **6**, the photoactive probe that exhibits the chromophore at the longest distance from the surface, revealing that "diving" at the sixteen bond distance leads to a quenching rate constant *ca.* one order of magnitude lower than the value found in solution. This fact clearly indicates that MNP can still be quenched by iodide but to a much lesser extent. In all cases results from steady-state and time-resolved experiments were comparable, as a proof of the dynamic nature of the processes.

Moreover, Fig. 3A clearly illustrates the decreasing tendency of the slope of the Stern–Volmer plots for iodide quenching from **1** to **6** in MM. In particular, the specific rate constants (k_q) obtained for **1–6** from time-resolved experiments in MM are shown in Table 1. The steady-state measurements gave very similar values for the quenching rate constants and revealed the same trends (the specific values are shown in ESI page S28†). A consistent decrease in the quenching constants was found in parallel with increasing spacer length. Overall, the deeper the MNP chromophore is incorporated into MM, the less accessibility to iodide exhibits.

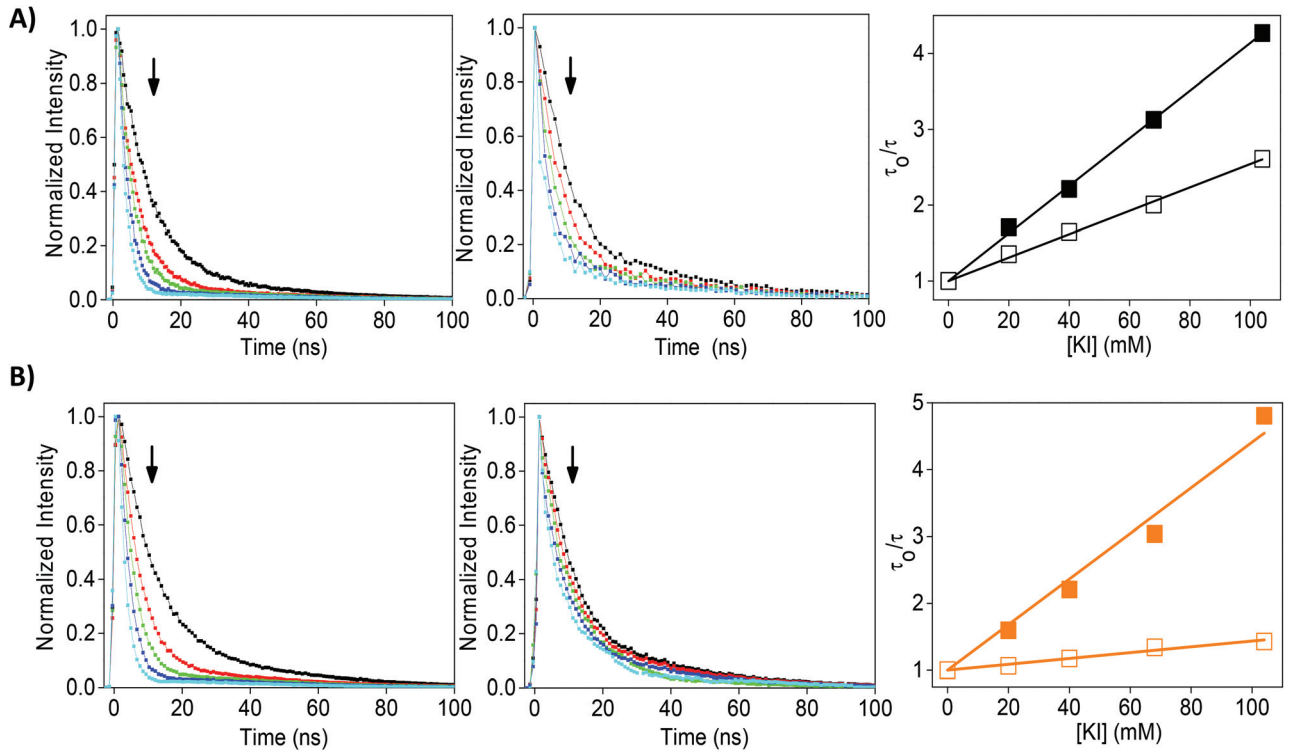

Fig. 2 Changes in the emission decay traces (λ_{exc} = 295 nm) of **1** (A) and **6** (B) upon addition of increasing amounts of KI (0–104 mM), in aqueous NaCl 0.2 M (left) and inside MM (middle). Right column: Corresponding Stern–Volmer plots in solution (solid squares) and in MM (blank squares).

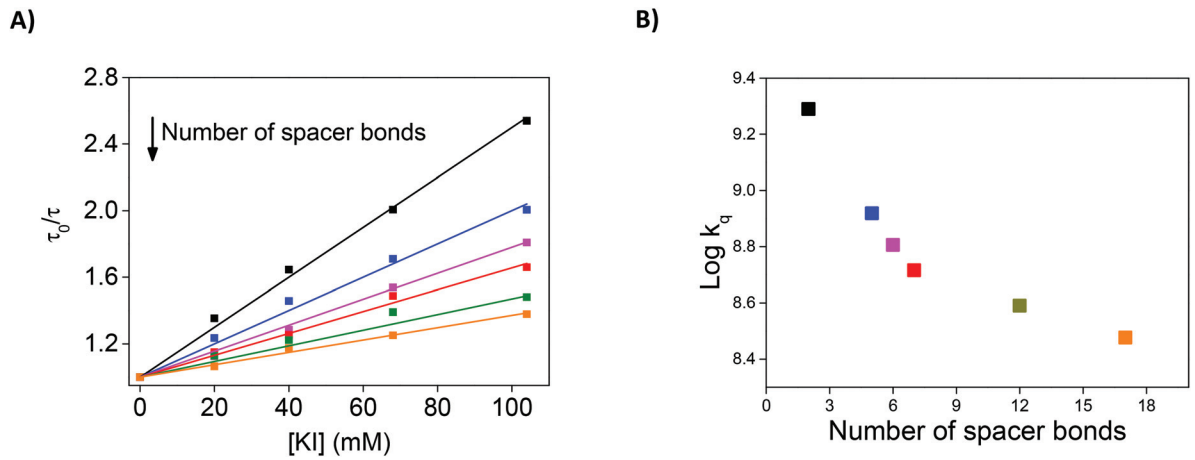

Fig. 3 (A) Stern–Volmer plots obtained for the iodide fluorescence quenching of the photoactive derivatives; (B) plots of the apparent quenching rate constants ($\log k_q$) *vs.* number of spacer bonds. All the experiments were run within MM containing the appropriate probe (**1**, **2**, **3**, **4**, **5** and **6**) under time-resolved conditions.

By contrast, in solution, all values were in the same range $(3.00 \pm 0.15) \times 10^9$ M^{-1} s^{-1} indicating that the behavior of the chromophore is independent of the length of the attached chain (see ESI page S28† for the specific experimental values determined for **1**–**6**). It is worth noting that the decrease by one order of magnitude found in the apparent quenching rate constants for **6** from solution to MM is in agreement with the recently reported lowering observed for naproxen methyl ester when incorporated into MM.[4] Even more revealing was to plot the apparent quenching rate constants ($\log k_q$) *versus* the number of spacer bonds. As is shown in Fig. 3B, these values exhibited an initial sharp decrease that after seven bonds follows a milder trend. A non-linear behaviour has previously been observed for the quenching of pyrene fluorescence by TEMPO in oil–water emulsions, which has been attributed to a cut-off effect.[21] In our case, the non-linear behaviour leads

Table 1 Dynamic rate constants ($k_q \times 10^{-9}/M^{-1}\ s^{-1}$) for iodide fluorescence quenching of **1–6** in MM[a]

MNP probe	$k_q \times 10^{-9}/M^{-1}\ s^{-1}$	$\log k_q$
1	1.98 ± 0.03	9.29
2	0.83 ± 0.03	8.92
3	0.65 ± 0.01	8.81
4	0.52 ± 0.08	8.72
5	0.39 ± 0.05	8.59
6	0.30 ± 0.05	8.47

[a] Each rate constant is the average of three independent time-resolved runs.

only to a decrease in the slope (plot of Fig. 5B) and seems more consistent with the shell–core model.

The observed dynamic quenching could be attributed to the photoinduced electron transfer from I^- to the MNP singlet excited state. Indeed, this operating mechanism is one of the most likely and thermodynamically feasible mechanisms taking into account the values of the involved redox potentials and the singlet energy of MNP (see estimations in ESI, page S33†). As a matter of fact, the detection of triiodide as the final product, upon steady-state photolysis, was straightforward and constituted an unambiguous mechanistic proof (Fig. 4). Thus, as representative examples, **1**, **4** and **5** were incorporated into the MM, and the electron transfer reaction from iodide was monitored by UV-vis (see Fig. 4A for the formation of I_3^- in the case of **1**, and Fig. 4B for the kinetics of the three examples). In all cases, the appearance of two new absorption bands with maxima at 290 and 360 nm attributable to I_3^- was clearly observed. As detailed in the inset of Fig. 4A, these bands result from the oxidation of iodide, eventually forming triiodide, as a proof of the electron transfer process.[32,33] When kinetics of the photo-redox reactions were plotted all together the observed trend for the formation of I_3^- (**1** > **4** > **5**) was also witnessed in agreement with the lower penetration capability of I^- with depth, and therefore with the spacer length.

Hence, the kinetics of I_3^- formation can be correlated with fluorescence quenching constants, providing a second channel of measurements for the photoactive bathymeter and demonstrating that the depth of a chromophore in MM may have clear implications in the reactivity.

Having designed and synthesized the bathymeter toolbox, measurements were performed on a selection of compounds exhibiting the same MNP unit but not anchored to the floating beacon (**7–13**, Chart 2). Their encapsulation into MM was achieved in one pot, as described above for **1–6**, and the quenching extent of their MNP unit by iodide was investigated by means of steady-state and time-resolved fluorescence experiments. The determined rate constants for all of them are shown in Table 2 and ESI.† The Stern–Volmer plots obtained for several selected compounds (**1**, **7**, **8**, **9** and **10**) are also shown in Fig. 5A (see page S31 in the ESI† for all steady-state and time-resolved quenching experiments for **7–13**). The obtained $\log k_q$ values were extrapolated between the experimental data determined with the probes **1–6** used to build the bathymeter (see Fig. 3B). It should be noted that the direct comparison with **1–6** (Fig. 5B) revealed that **8** and **9** remained relatively close to the surface ("snorkelling"), while **7**, **10–13** "dived" much deeper into the MM. Although these results were not unexpected, especially for **9**, **12** or **13**, a parallel

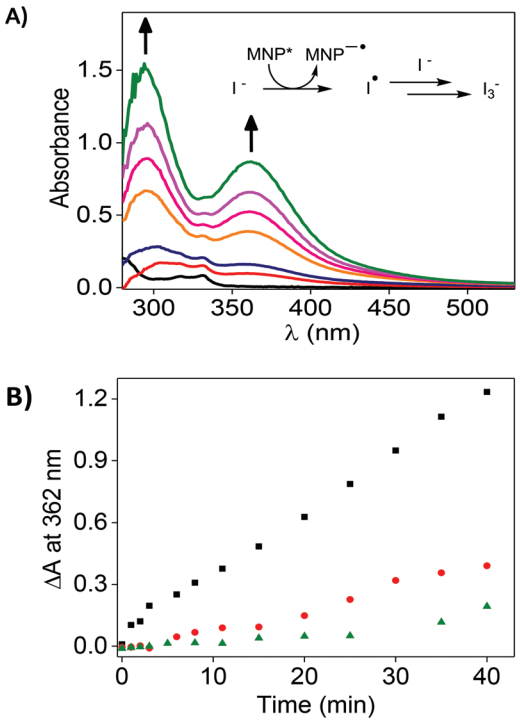

Fig. 4 (A) UV-vis spectra recorded at different reaction times (0, 11, 15, 25, 35, 40 min) for **1** within MM in the presence of KI (104 mM). Inset: Reaction mechanism. (B) Kinetics of the photoinduced electron transfer reactions monitored at 362 nm for **1** (black), **4** (red) and **5** (green).

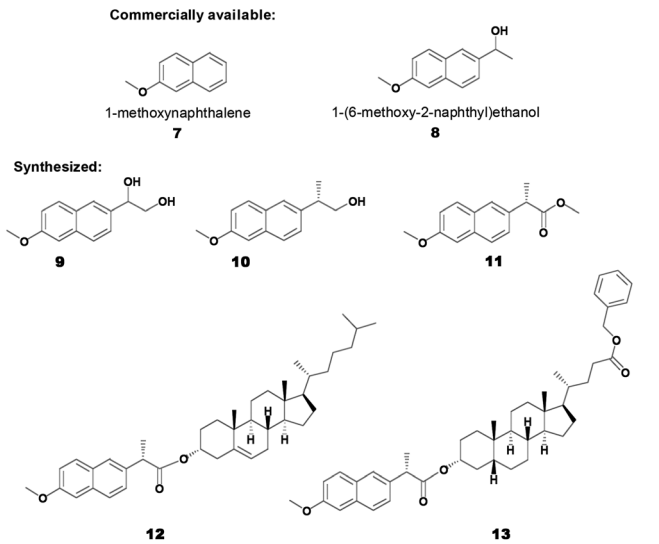

Chart 2 MNP derivatives used to test the designed and built bathymeter.

Table 2 Dynamic rate constants for iodide fluorescence quenching of **7–13** in MM[a]

NMP derivative	$k_q \times 10^{-9}/M^{-1}\ s^{-1}$	$\log k_q$
7	0.27 ± 0.02	8.43
8	0.65 ± 0.03	8.81
9	1.09 ± 0.02	9.03
10	0.28 ± 0.02	8.44
11	0.27 ± 0.04	8.43
12	0.07 ± 0.002[b]	7.89[b]
13	0.08 ± 0.004[b]	7.82[b]

[a] Each rate constant is the average of three independent time-resolved runs. [b] Value was obtained from steady-state experiments.

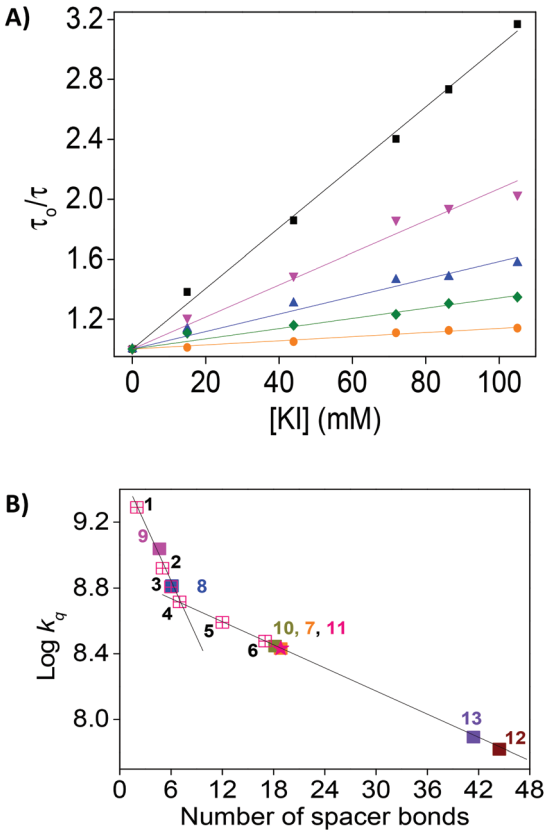

Fig. 5 (A) Stern–Volmer plots obtained for the time-resolved iodide fluorescence quenching of **1**, **7**, **8**, **9** and **10**; (B) plots of the quenching rate constants ($\log k_q$) *vs.* "number of spacer bonds" together with the data found from **1** to **6** (blank squares) used to build the bathymeter as shown in Fig. 3B. All data were obtained within MM containing the appropriate probe under time-resolved conditions.

control of the lipophilicity of these derivatives was still needed to validate the usefulness and scope of the bathymeter.

A general methodology for the determination of lipophilicity of organic compounds with a variety of structures is based on the widely accepted octanol–water partition coefficient (K_{ow}).[34] Nevertheless, the employed derivatives exhibited very limited solubility in octanol–water mixtures. To overcome this hurdle, the protocol was modified and octanol was changed to

Table 3 Determined K_{pw} (partition coefficient, pentane : water) calculated as A_{262} P/(A_{262} W + A_{262} P), and R_f calculated from TLC (hexane/ethyl acetate 1 : 0.6) for **1** and **7–13**[a]

NMP derivative	K_{pw}	R_f
1	0.57	0.20
7	0.97	0.86
8	0.76	0.46
9	n.d	0.08
10	0.89	0.41
11	0.89	0.77
12	0.97	0.92
13	0.94	0.87

[a] See TLC photo in ESI, page S36.

pentane. Thus, this experiment provided insights into the lipophilicity of the MNP derivatives.

A modified partition coefficient (K_{pw}) was defined as the relative concentration of the MNP derivatives in the organic (P) *versus* aqueous (W) phases, and were determined as A_{262} P/(A_{262} W + A_{262} P). In Table 3 are shown the determined K_{pw} values, and in ESI, page S35,† the complete UV-visible spectra of the organic and aqueous phases in each experiment are shown. As a general trend, analogous results were found from the partition coefficient using pentane/aqueous mixtures and from the iodide quenching. Due probably to the intramolecular H-bonding, it was not possible to determine K_{pw} of **9** and its depth was assigned based on fluorescence quenching. These complementary results were taken as a further confirmation of the usefulness and scope of the bathymeter.

As a complementary experiment, the retention factor (R_f, Table 3) of the MNP derivatives was determined using standard thin-layer chromatography on a sheet of aluminium covered by silica, and hexane/ethyl acetate (1 : 0.6) as the mobile phase (see picture in ESI, page S36†). This approach provided a parallel indication of lipophilicity which was qualitatively consistent with the k_q and K_{pw} scales.

Interestingly, the lipophilicity results obtained from: (i) the iodide quenching (Table 2 and Fig. 5B); (ii) the partition coefficient K_{pw} using pentane/aqueous mixtures (Table 3) and (iii) the retention factor, R_f, calculated from TLC (hexane/ethyl acetate 1 : 0.6) (Table 3), have been plotted all together and a good correlation has been observed (Fig. 6).

Experimental

Materials

(*S*)-Naproxen (NPX), glycine methyl ester hydrochloride, β-alanine methyl ester hydrochloride, methyl 4-aminobutyrate hydrochloride, 1-(6-methoxy-2-naphthyl)ethanol, 2-methoxy-6--vinylnaphthalene, lithocholic acid, cholesterol (Ch), egg lecithin from fresh egg yolk (L), and sodium cholate (NaCh) were commercially available. Milli-Q grade water (Merck) was used for sample preparation. Commercial solvents and reagents were used without further purification. The ^{1}H and

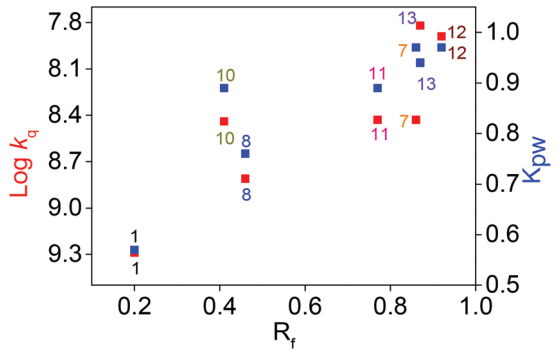

Fig. 6 Dynamic rate constants for iodide fluorescence quenching (log k_q, left) and partition coefficient (pentane : water) (K_{pw}, right) *versus* R_f, for **1**, **7**, **8**, **10**, **11**, **12** and **13**.

^{13}C NMR spectra were recorded by means of a Bruker (Rheinstetten, Germany) 300 MHz instrument; $CDCl_3$ and CD_3OD were used as solvents.

Synthesis of photoactive MNP probes 2–6. General procedure

N-(3-Dimethylaminopropyl)-*N*′-ethylcarbodiimide (EDC) was added to an anhydrous CH_2Cl_2 solution of the corresponding acid and the reaction mixture was cooled to 0 °C. Next, a solution of the pertinent amine, *N*,*N*-diisopropyl-*N*-ethylamine (DIEA) and 4-pyrrolidylpyridine (4-Pr-Py) in anhydrous CH_2Cl_2 was added dropwise under an inert atmosphere, and the reaction mixture was stirred overnight at rt. The reaction mixture was quenched upon addition of water and extracted with CH_2Cl_2. The corresponding ester was obtained after purification by column chromatography. Then, the ester was dissolved in MeOH and treated overnight with KOH at rt. The corresponding carboxylic acid was obtained after column purification. Detailed synthesis and characterization of compounds **2** to **6** can be found in the ESI (pages S4–S19†).

Synthesis of MNP-derivatives

Synthesis of 1-(6-methoxy-2-naphthalenyl)-1,2-ethanediol (9). 2-Methoxy-6-vinylnaphthalene (500 mg, 2.71 mmol, 1 eq.) was added to a mixture of *N*-methylmorpholine *N*-oxide (640 mg, 5.42 mmol, 2 eq.) and osmium tetroxide (40 mg, 0.15 mmol, 0.06 eq.) in THF : *tert*-butanol : water (10 : 10 : 4, 48 mL) and the mixture was stirred at 40 °C for 24 h. Afterwards, the solution was cooled in an ice bath, and quenched upon the addition of sodium sulfite (676 mg, 5.42 mmol, 2 eq.). After stirring for 30 min, the mixture was poured into water (50 mL) and extracted with CH_2Cl_2 (×3). The combined organic layers were dried over $MgSO_4$, filtered and concentrated under vacuum. The expected compound **9** (545 mg, 92%) was purified by column chromatography (CH_2Cl_2/MeOH, 99.5 : 0.5). Mp: 154–155 °C. ^1H NMR (300 MHz, CD_3OD): δ 3.70 (m, 2H, CH_2OH), 3.90 (s, 3H, OCH_3), 4.81 (m, 1H, CHOH), 7.11 (dd, J = 9 and 3 Hz, 1H, Ar–H), 7.21 (d, J = 3 Hz, 1H, Ar–H), 7.46 (dd, J = 9 and 3 Hz, 1H, Ar–H), 7.72–7.76 (m, 3H, Ar–H); ^{13}C NMR (75 MHz, CD_3OD): δ 55.7 (CH_3), 68.7 (CH_2), 76.1 (CH), 106.7 (CH), 119.8 (CH), 126.1 (CH), 127.9 (CH), 130.2 (C), 130.4 (CH), 135.7 (C), 138.4 (C), 159.2 (C). Exact mass: m/z found 218.0940, calculated for $C_{13}H_{14}O_3$ (MH^+) 218.0943.

Synthesis of 2(*R*)-(6-methoxynaphthalen-2-yl)propan-1-ol (10). HOBt·H_2O (319 mg, 2.36 mmol, 1.1 eq.) and EDC·HCl (453 mg, 2.36 mmol, 1.1 eq.) were added to a solution of (*R*)-naproxen (500 mg, 2.17 mmol, 1 eq.) in CH_2Cl_2 (22 mL). The mixture was stirred for 30 min and then concentrated under vacuum. The residue was redissolved in THF (22 mL), cooled to 0 °C, and $NaBH_4$ (178 mg, 4.72 mmol, 2.2 eq.), followed by H_2O (3 mL) were added. The resulting mixture was stirred at 0 °C for further 30 min, and then quenched with MeOH (7.5 mL). Then, ethyl acetate (25 mL) was added, and the organic phase was successively washed with aqueous solutions of 10% citric acid (×2), 10% $NaHCO_3$ (×2), 10% K_2CO_3 (×2) and brine (×2), and then it was dried over $MgSO_4$ and concentrated under vacuum. The crude was purified by column chromatography (CH_2Cl_2/ethyl acetate, 85 : 15) to obtain **10** as a white solid (330 mg, 70%). Mp: 97–99 °C. ^1H NMR (300 MHz, $CDCl_3$): δ 1.29 (d, J = 6 Hz, 3H, CH_3), 3.06–3.13 (m, 1H, CH), 3.78 (d, J = 6 Hz, 2H, CH_2OH), 3.92 (s, 3H, OCH_3), 7.12–7.16 (m, 2H, Ar–H), 7.35 (dd, J = 6 and 3 Hz, 1H, Ar–H), 7.61 (s, 1H, Ar–H), 7.69–7.72 (m, 2H, Ar–H); ^{13}C NMR (75 MHz, $CDCl_3$): δ 17.6 (CH_3), 42.4 (CH), 55.3 (CH_3), 68.7 (CH_2), 105.6 (CH), 118.9 (CH), 125.9 (CH), 126.3 (CH), 127.2 (CH), 129.0 (C), 129.1 (CH), 133.6 (C), 138.7 (C), 157.5 (C). Exact mass: m/z found 216.1145, calculated for $C_{14}H_{16}O_2$ (MH^+) 216.1150.

Synthesis of (*S*)-naproxen methyl ester (11). Synthesis of this compound was described elsewhere.[30] Briefly, a methanolic solution (7 mL) of (*S*)-naproxen (500 mg, 2.17 mmol) was heated at 80 °C, and H_2SO_4 (0.1 mL) was added carefully, and the reaction mixture was refluxed for 8 h. After cooling to room temperature, aqueous saturated $NaHCO_3$ was added and the ester was extracted with ethyl acetate (×3), dried over $MgSO_4$ and concentrated under reduced pressure to yield the naproxen methyl ester as a white solid (quantitative). Mp: 96–99 °C. ^1H NMR (300 MHz, $CDCl_3$): δ 1.61 (d, J = 6 Hz, 3H, CH_3), 3.66 (s, 3H, $COOCH_3$), 3.88 (m, 1H, CH), 3.93 (s, 3H, OCH_3), 7.13–7.19 (m, 2H, Ar–H), 7.43 (dd, J = 9 and 3 Hz, 1H, Ar–H), 7.69–7.74 (m, 3H, Ar–H); ^{13}C NMR (75 MHz, $CDCl_3$): δ 18.6 (CH_3), 45.4 (CH), 52.05 (CH_3), 55.3 (CH_3), 105.6 (CH), 119.0 (CH), 125.9 (CH), 126.2 (CH), 127.2 (CH), 129.0 (C), 129.3 (CH), 133.7 (C), 135.7 (C), 157.7 (C), 175.2 (CO). Exact mass: m/z found 244.1092, calculated for $C_{15}H_{16}O_3$ (MH^+) 244.1099.

Synthesis of 3α-(*S*)-NPX-Ch (12). Synthesis of this compound was described elsewhere.[29] ^1H and ^{13}C NMR spectra are shown in the ESI.†

Synthesis of 3α-(*S*)-NPX-LC-Bn (13). To a cold solution of lithocholic acid (0.45 g, 1.2 mmol, 1 eq.) in anhydrous DMF (5 mL), DBU (0.2 mL, 1.35 mmol, 1.1 eq.) was added, and the mixture was stirred at 0 °C for 10 min. Then, benzyl bromide (0.16 mL, 1.35 mmol, 1.1 eq.) was added and the mixture was stirred overnight at rt. Afterwards, the solvent was evaporated, and the mixture was redissolved in ethyl acetate (2 mL). The organic layer was washed with saturated $NaHCO_3$, 1 M HCl,

and brine, dried over $MgSO_4$ and concentrated under reduced pressure. The crude was purified by column chromatography (ethyl acetate : *n*-hexane, 40 : 60) to give LC-Bn (520 mg, 1.12 mmol, 93%) that was used in the following step without further characterization. To a stirred solution of LC-Bn (340 mg, 0.73 mmol, 1 eq.) and TBTU (280 mg, 0.87 mmol, 1.2 eq.) in anhydrous DMF (3 mL), (*S*)-NPX (200 mg, 0.80 mmol, 1.1 eq.) in anhydrous DMF (2 mL) followed by DIEA (0.38 mL, 2.18 mmol, 3 eq.) were added dropwise and then the reaction mixture was allowed to react at rt for 6 h. Afterwards, it was poured into brine and extracted with dichloromethane; the combined organic layers were washed with brine, dried over $MgSO_4$ and concentrated under reduced pressure. The crude was purified by column chromatography (ethyl acetate : *n*-hexane, 90 : 10) to give compound **13** (400 mg, 0.58 mmol, 80%). ^{1}H NMR (300 MHz, $CDCl_3$): δ 0.64 (s, 3H, CH_3), 0.93 (s, 6H, 2 × CH_3), 1.04–1.41 (complex signal, 18H), 1.41 (d, J = 7.2 Hz, 3H, CH_3), 1.75–1.95 (complex signal, 8H), 2.27–2.49 (m, 2H, CH), 3.84 (q, J = 7.2 Hz, 1H, CH), 3.93 (s, 3H, OCH_3), 4.74–4.82 (m, 1H, CH), 5.15 (d, J = 1.9 Hz, 2H, CH_2), 7.14–7.18 (m, 2H, Ar–CH), 7.30–7.47 (m, 6H, Ar–CH), 7.65 (d, J = 1.2 Hz, 1H), 7.69 (dd, J = 8.4 Hz and 2.6 Hz, 2H, Ar–CH); ^{13}C NMR (75 MHz, $CDCl_3$): δ 12.0 (CH_3), 18.3 (CH_3), 18.8 (CH_3), 20.8 (CH_2), 23.3 (CH_3), 24.2 (CH_2), 26.3 (CH_2), 27.1 (CH_2), 28.2 (CH_2), 31.0 (CH_2), 31.3 (CH_2), 34.6 (C), 35.0 (CH_2), 35.3 (CH), 35.7 (CH), 35.8 (CH), 40.0 (CH_2), 40.4 (CH), 41.9 (CH), 42.0 (C), 42.7 (CH), 45.7 (CH), 45.8 (CH), 55.3 (CH_3), 56.0 (CH_2), 56.3 (CH_2), 56.4 (CH), 66.1 (CH_2), 74.7 (CH), 105.6 (CH), 118.9 (CH), 125.9 (CH), 126.0 (CH), 126.2 (CH), 128.2 (CH), 128.6 (CH), 129.0 (CH), 129.3 (CH), 133.6 (C), 136.1 (CH), 136.2 (C), 157.6 (C), 174.1 (C=O), 174.2 (C=O). Exact mass: m/z found 701.4161, calculated for $C_{45}H_{58}O_5Na$ (MH^+) 701.4182.

Fluorescence quenching experiments

In a typical quenching experiment the appropriate volumes of a freshly prepared KI in 0.2 M NaCl solution (2 M) were added to the aerated photoactive probes (2×10^{-5} M) in 0.2 M NaCl or within MM. Emission measurements were performed upon excitation of the probe at 290 nm (steady-state measurements) or 295 nm (time-resolved experiments) at room temperature using 10 × 10 mm quartz cells of 4 mL capacity. The kinetic traces were fitted to logarithmic decay functions.

Photo-redox experiments

Freshly prepared and rehydrated MM, containing the photoactive probes (2×10^{-5} M) and KI (104 mM) were irradiated with a monochromatic lamp at 330 nm for 40 minutes, and the evolution of the formation of I_3^- was monitored by UV. Blank experiments were performed irradiating MM without the photoactive probes in the presence of KI.

Partition coefficient experiments

The solubility of the MNP derivatives (**1**, **7**–**13**) was assessed from the mixture pentane/water. In a typical experiment a well-known amount of each probe was weighed to achieve a concentration of 0.152 mM in pentane (solution P). This solution P was stirred for 24 h before the UV spectra were recorded. Then 25 mL of solution P were mixed with 25 mL of water and the mixture was stirred for further 2 h. Then the two phases were separated, and the corresponding UV spectra of both were recorded. The absorbance of the two phases at 262 nm was used to determine the K_{pw}.

Conclusions

We have designed and built a photoactive bathymeter that contains a carboxylic acid moiety and a signalling MNP chromophore covalently attached to each other through a spacer. The carboxylic acid moiety "floats" on the surface, while the spacer has a fixed length between one and sixteen bonds to allow the MNP for "snorkelling" or "diving" within MM. Quenching of the singlet excited state of the MNP chromophore by iodide is dynamic in nature; its rate constants (k_q) show a remarkable decrease with spacer length indicating their dependence on the distance the signalling chromophore can "dive" in MM. The spectral signature of I_3^- upon steady-state photolysis acts as an unequivocal proof of the electron transfer process and its formation and growth reveal that the chemical reactivity markedly depends on the location inside the MM. The role of the lipophilic characteristic of the different MM regions in the results has been confirmed by comparison of the k_q values with two established scales, namely a modified partition coefficient and the retention factor in thin layer chromatography. The photoactive bathymeter has been successfully tested for a series of compounds containing the MNP chromophore but not anchored to the floating beacon. This concept could in principle be extended to a variety of microheterogeneous systems and membrane models.

Conflicts of interest

There are no conflicts to declare.

Acknowledgements

Financial support from the Spanish Government (SEV-2016-0683), Red RETICS de Investigación de Reacciones Adversas a Alérgenos y Fármacos (RIRAAF), Instituto de Salud Carlos III (RD012/0013, RD16/0006/0030, FIS PI16/01877), VLC-Campus and the Generalitat Valenciana (Prometeo Program) is gratefully acknowledged.

References

1 C. J. H. Porter, N. L. Trevaskis and W. N. Charman, *Nat. Rev. Drug Discovery*, 2007, **6**, 231–248.
2 M. A. Hammad and B. W. Muller, *Eur. J. Pharm. Biopharm.*, 1998, **46**, 361–367.

3 S. Nagadome, O. Numata, G. Sugihara, Y. Sasaki and H. Igimi, *Colloid Polym. Sci.*, 1995, **273**, 675–680.
4 A. F. Hofmann, *Arch. Intern. Med.*, 1999, **159**, 2647–2658.
5 J. J. Ding, Y. J. Sun, J. F. Li, H. M. Wang and S. R. Mao, *J. Drug Targeting*, 2017, **25**, 532–540.
6 D. D. Lasic, *Nature*, 1992, **355**, 279–280.
7 L. Cheng, A. Kamkaew, H. Y. Sun, D. W. Jiang, H. F. Valdovinos, H. Gong, C. G. England, S. Goel, T. E. Barnhart and W. B. Cai, *ACS Nano*, 2016, **10**, 7721–7730.
8 C. A. Lipinski, F. Lombardo, B. W. Dominy and P. J. Feeney, *Adv. Drug Delivery Rev.*, 1997, **23**, 3–25.
9 K. Beaumont, E. Schmid and D. A. Smith, *Bioorg. Med. Chem. Lett.*, 2005, **15**, 3658–3664.
10 M. S. Al-Abdul-Wahid, C. Neale, R. Pomès and R. S. Prosser, *J. Am. Chem. Soc.*, 2009, **131**, 6452–6459.
11 M. Afri, A. A. Frimer and Y. Cohen, *Chem. Phys. Lipids*, 2004, **131**, 123–133.
12 Y. Cohen, E. Bodner, M. Richman, M. Afri and A. A. Frimer, *Chem. Phys. Lipids*, 2008, **155**, 98–113.
13 Y. Cohen, M. Afri and A. A. Frimer, *Chem. Phys. Lipids*, 2008, **155**, 114–119.
14 M. Afri, C. Alexenberg, P. Aped, E. Bodner, S. Cohen, M. Ejgenburg, S. Eliyahu, P. Gilinsky-Sharon, Y. Harel, M. E. Naqqash, H. Porat, A. Ranz and A. A. Frimer, *Chem. Phys. Lipids*, 2014, **184**, 105–118.
15 M. Afri, M. E. Naqqash and A. A. Frimer, *Chem. Phys. Lipids*, 2011, **164**, 759–765.
16 E. Bodner, M. Afri and A. A. Frimer, *Free Radicals Biol. Med.*, 2010, **49**, 427–436.
17 M. Laguerre, L. J. L. Giraldo, J. Lecomte, M. C. Figueroa-Espinoza, B. Barea, J. Weiss, E. A. Decker and P. Villeneuve, *J. Agric. Food Chem.*, 2009, **57**, 11335–11342.
18 M. Laguerre, L. J. L. Giraldo, J. Lecomte, M. C. Figueroa-Espinoza, B. Barea, J. Weiss, E. A. Decker and P. Villeneuve, *J. Agric. Food Chem.*, 2010, **58**, 2869–2876.
19 C. Aliaga, F. Bravo-Moraga, D. Gonzalez-Nilo, S. Marquez, S. Luhr, G. Mena and M. C. Rezende, *Food Chem.*, 2016, **192**, 395–401.
20 C. Aliaga, A. L. de Arbina and M. C. Rezende, *Food Chem.*, 2016, **206**, 119–123.
21 A. L. de Arbina, M. C. Rezende and C. Aliaga, *Food Chem.*, 2017, **224**, 342–346.
22 P. Agostinis, K. Berg, K. A. Cengel, T. H. Foster, A. W. Girotti, S. O. Gollnick, S. M. Hahn, M. R. Hamblin, A. Juzeniene, D. Kessel, M. Korbelik, J. Moan, P. Mroz, D. Nowis, J. Piette, B. C. Wilson and J. Golab, *CA-Cancer J. Clin.*, 2011, **61**, 250–281.
23 A. Kamkaew, S. H. Lim, H. B. Lee, L. V. Kiew, L. Y. Chung and K. Burgess, *Chem. Soc. Rev.*, 2013, **42**, 77–88.
24 S. Yano, S. Hirohara, M. Obata, Y. Hagiya, S. Ogura, A. Ikeda, H. Kataoka, M. Tanaka and T. Joh, *J. Photochem. Photobiol., C*, 2011, **12**, 46–67.
25 D. Dolmans, D. Fukumura and R. K. Jain, *Nat. Rev. Cancer*, 2003, **3**, 380–387.
26 I. Bronshtein, M. Afri, H. Weitman, A. A. Frimer, K. M. Smith and B. Ehrenberg, *Biophys. J.*, 2004, **87**, 1155–1164.
27 A. Lavi, H. Weitman, R. T. Holmes, K. M. Smith and B. Ehrenberg, *Biophys. J.*, 2002, **82**, 2101–2110.
28 A. Chattopadhyay and E. London, *Biochemistry*, 1987, **26**, 39–45.
29 E. Nuin, M. Gomez-Mendoza, I. Andreu, M. L. Marin and M. A. Miranda, *Org. Lett.*, 2013, **15**, 298–301.
30 E. Nuin, M. Gomez-Mendoza, M. L. Marin, I. Andreu and M. A. Miranda, *J. Phys. Chem. B*, 2013, **117**, 9327–9332.
31 M. Gomez-Mendoza, E. Nuin, I. Andreu, M. L. Marin and M. A. Miranda, *J. Phys. Chem. B*, 2012, **116**, 10213–10218.
32 G. Boschloo and A. Hagfeldt, *Acc. Chem. Res.*, 2009, **42**, 1819–1826.
33 J. M. Gardner, M. Abrahamsson, B. H. Farnum and G. J. Meyer, *J. Am. Chem. Soc.*, 2009, **131**, 16206–16214.
34 J. Sangster, *J. Phys. Chem. Ref. Data*, 1989, **18**, 1111–1229.